remote sensing

MDPI

Communication

A Potential Mechanism of the Satellite Thermal Infrared Seismic Anomaly Based on Change in Temperature Caused by Stress Variation: Theoretical, Experimental and Field Investigations

Peixun Liu, Shunyun Chen *, Qiongying Liu, Yanshuang Guo, Yaqiong Ren, Yanqun Zhuo and Jiahui Feng

State Key Laboratory of Earthquake Dynamics, Institute of Geology, China Earthquake Administration, Beijing 100029, China
* Correspondence: chenshy@ies.ac.cn

Abstract: Satellite thermal infrared remote sensing has received worldwide attention in earthquake-precursors exploration. Meanwhile, it has also encountered great controversy due to the lack of quantitative interpretation of the observations, despite the existing qualitative physical mechanisms being able to greatly help us understand thermal infrared anomalies. Here, we report a potential mechanism to quantitatively analyze co-seismic thermal infrared anomalies based on temperature change caused by stress variation through theoretical, experimental, and field investigations. This paper firstly deduces theoretically the temperature variation during elastic deformation of rock on the basis of the thermodynamic theory. Secondly, three laboratory experiments on rock samples are conducted to verify the theoretical estimates of the temperature changes caused by stress variations using an infrared camera with the spectral range of 8~12 μm. Thirdly, a mechanical model on thrust faults is built to evaluate the co-seismic temperature drop as a result of thrust faulting. The model shows that the co-seismic temperature drop in rocks should be in the order of 0.18 K. This variation in rock temperature may cause a change in heat equivalent to changes in shallow atmospheric temperatures of 3.0–6.0 K, which is in accordance with the temperature anomalies observed by satellite thermal infrared remote sensing. In addition, the temperature change caused by crustal stress variation may involve a large spatial scale, covering the whole focal area, which has characteristics of regional distribution and is conducive to satellite observation. Therefore, a quantitative explanation of the satellite thermal infrared seismic anomaly mechanism can be given via the temperature change caused by crustal stress variation.

Keywords: satellite thermal infrared remote sensing; land surface temperature (LST); thrust faulting; co-seismic temperature drop; co-seismic stress drop

Citation: Liu, P.; Chen, S.; Liu, Q.; Guo, Y.; Ren, Y.; Zhuo, Y.; Feng, J. A Potential Mechanism of the Satellite Thermal Infrared Seismic Anomaly Based on Change in Temperature Caused by Stress Variation: Theoretical, Experimental and Field Investigations. *Remote Sens.* **2022**, *14*, 5697. https://doi.org/10.3390/rs14225697

Academic Editors: Chun Zhu, Shibin Tang, Yujun Zuo and Qian Yin

Received: 17 September 2022
Accepted: 8 November 2022
Published: 11 November 2022

1. Introduction

Satellite thermal infrared remote sensing has received worldwide attention in earthquake-precursor exploration. Over recent decades, thermal anomalies prior to large earthquakes, which have been observed by satellite thermal infrared remote sensing and are thought to have the potential for earthquake forecasting, have been intensively reported [1–17]. Significant linkages between pre-seismic signals and upcoming earthquakes have been identified statistically in retrospective studies of global earthquakes by using a variety of anomaly analytical methods [14–16]. Seemingly, satellite remote sensing techniques have become an effective approach to monitoring pre-seismic processes along active fault zones [11,12,14,16].

In spite of the statistical evidence of the detected pre-seismic signal, pre-monitoring information before earthquakes has not been so far properly explained by a sufficiently accurate model. The observed thermal infrared anomalies can be explained by several

mechanisms [18]. Specifically, the thermal inferred anomalies have often been interpreted as (1) deflation of gases such as CO_2 and CH_4 within the crust [19], (2) p-hole excitation generated by earthquake activities [20,21], (3) energy conversion between mechanics and heat [22–24], and (4) systematic coupling effects, such as seismic atmosphere–ionosphere coupling [6,25]. These physical mechanisms are associated with stress changes or their secondary effects, but each mechanism emphasizes different aspects that are produced by stress changes or accompany stress changes, such as gas, electricity, magnetism, or heat.

In general, the above physical mechanisms, which were derived from different experimental results, were mainly conceptual models. As a result, quantitative interpretations for the satellite thermal infrared anomalies cannot be obtained based on these models. Thus, in order to understand the underlying physical process of satellite thermal infrared anomalies, it is necessary and important to carry out quantitative analysis through these mechanisms. Recently, Carbone et al. (2021) [12] offered an analytical-quantitative model for land temperature anomalies based on the coupling between the lithosphere and the atmosphere, which describes how the pressure and density disturbance in the lower atmosphere is generated by earthquake-induced ground motion.

On the other hand, the relation between temperature change and stress variation could provide some clues to this issue. Previous laboratory studies suggest that temperature is sensitive to stress changes [21,23,26–32]. Moreover, temperature changes generated by the mechanical effects have also been investigated, in both laboratory and field, in rock-engineering or thermal surveys [32–34]. In addition, co-seismic temperature changes near seismogenic faults were quickly measured via deep drilling after earthquakes. For instance, the temperature of the seismogenic faults increased by 0.06 K, 0.03 K, and 0.31 K during the Mw7.6 Chi-Chi earthquake in 1999 [35], the Mw7.9 Wenchuan earthquake in 2008 [27], and the Mw9.0 Tohoku-Oki earthquake in 2011 [36], respectively. Interestingly, these observations suggest that the co-seismic temperature changes in the fault zone are lower than the expected temperature changes due to frictional heating, implying that such negative temperature anomalies may be caused by stress unloading of the crustal rocks during the occurrence of the earthquakes [28,29]. Thus, the temperature change caused by stress variation is possibly a key approach to the quantitative understanding of satellite thermal infrared seismic anomalies.

This paper at first introduces a thermodynamic theory on temperature variation during elastic deformation of rock and verifies the theoretical result through experiments on rock samples. Then, a stick-slip mechanical model on the thrust fault is built to analyze the temperature responses to co-seismic stress drops.

2. Thermodynamic Formulas for Solid Adiabatic Deformation

As mentioned above, the relationship between temperature and stress has been well studied. However, there are differences in stress conditions between laboratory and field. Namely, experiments in the laboratory are mainly conducted in uniaxial (1D) or biaxial (2D) stress states, while rocks are loaded under a three-dimensional (3D) stress state in the field. Such a discrepancy may cause confusion when experimental results are applied to the field if the physical meanings and mathematical logic of the relevant physical parameters are not sorted out to facilitate consistency.

Here, we simply introduce thermodynamic formulas for solid adiabatic deformation, so that the relationship between temperature response and stress change can be less difficultly applied to field exploration. In fact, many researchers suspect that elastic deformation may produce temperature changes, and they think this is not consistent with the law of conservation of energy. In general, elastic mechanics is based on the assumption that the condition is isothermal, thus the temperature in elastic mechanics is not related to the stress–strain. However, under non-isothermal conditions, temperature changes of solids can cause elastic deformation, and elastic deformation can contribute to temperature changes, which is the so-called thermo-elastic effect. The temperature response to the stress change is equivalent to the inverse problem of the thermal inflation. For heat-expanded material,

the temperature increases during the compression, and decreases under unloading. And temperature and stress changes simultaneously.

Based on the first and second laws of thermodynamics, as for the linear elastic body under adiabatic conditions, there is [37,38]

$$ds = \frac{c_\sigma}{T} dT + \left(\frac{\partial \varepsilon_{ij}}{\partial T}\right)_\sigma d\sigma_{ij} \quad (1)$$

where s is entropy per unit volume, c_σ is specific heat per unit mass at a constant stress, T is absolute temperature, ε_{ij} is the component of strain, and σ_{ij} is the component of stress.

Elastic deformation can be approximately regarded as a reversible process. As for the reversible process, according to the second law of thermodynamics, the entropy is constant, namely $ds = 0$. Under the assumption of small deformation, c_σ and $\left(\frac{\partial \varepsilon_{ij}}{\partial T}\right)_\sigma$ are constant. Compression is defined as positive in rock mechanics. For one dimensional questions, we have

$$\Delta T = \frac{T_0 \alpha_l}{\rho c_\sigma} \Delta\sigma \quad (2)$$

where ΔT is the increment of temperature, T_0 is the initial temperature, and $\alpha_l = -\left(\frac{\partial \varepsilon_{ij}}{\partial T}\right)_\sigma$ is the coefficient of linear thermal expansion at a constant stress. $\Delta\sigma$ is the increment of stress. In the case of uniaxial deformation, the temperature increases with the extrusion and decreases with the tension for a material with the coefficient of linear thermal expansion $\alpha_l > 0$, such as rock. The temperature change is synchronized with the stress change.

As for three dimensional problems, we can choose the principal axes as the coordinate axes; Equation (1) may be changed into

$$ds = \frac{c_\sigma}{T} dT + \left(\frac{\partial \varepsilon_{11}}{\partial T}\right)_\sigma d\sigma_{11} + \left(\frac{\partial \varepsilon_{22}}{\partial T}\right)_\sigma d\sigma_{22} + \left(\frac{\partial \varepsilon_{33}}{\partial T}\right)_\sigma d\sigma_{33} \quad (3)$$

As for isotropy material, $\left(\frac{\partial \varepsilon_{11}}{\partial T}\right)_\sigma = \left(\frac{\partial \varepsilon_{22}}{\partial T}\right)_\sigma = \left(\frac{\partial \varepsilon_{33}}{\partial T}\right)_\sigma$. Under the condition of small deformation, a new equation is obtained

$$\frac{\Delta T}{T_0} = \frac{3\alpha_l}{\rho c_\sigma} \Delta\left(\frac{\sigma_{11} + \sigma_{22} + \sigma_{33}}{3}\right) = \frac{\alpha_v}{\rho c_\sigma} \Delta\sigma_m \quad (4)$$

where, α_v is the coefficient of volumetric thermal expansion at a constant stress, approximately equal to three times the coefficient of linear thermal expansion when the deformation is small. σ_m is the mean stress (or the volumetric stress).

Equation (4) gives an interesting result that the temperature change during elastic deformation is only related to the mean stress, but not the deviator stress. For instance, for granite, $\alpha_v = 2.4 \times 10^{-5} K^{-1}$, $c_\sigma = 800 J/kg{\cdot}K$, and $\rho = 2670 kg/m^3$, and for sandstone, $\alpha_v = 3.0 \times 10^{-5}$, $c_\sigma = 930 J/kg{\cdot}K$, and $\rho = 2500 kg/m^3$ [39]. According to Equation (4), at room temperature $T_0 = 300$ K, the temperature decreases3.3 mK for granite and 3.9 mK for sandstone, respectively, when its mean stress decreases at 1.0 MPa. From these results, we can figure out that the value of temperature change generated by stress variation is very small. Generally, most rock materials show thermal expansion, and the thermal expansion coefficient, density and specific heat only change within the same order of magnitude. This is to say, the temperatures change of the rocks produced by the stress variation is in the level of the same order of magnitude.

3. Experiments on Temperature Variation and Elastic Deformation

To verify the theory mentioned above, we carried out a series of experiments in the laboratory. Ideally, the experiments should be performed under adiabatic conditions, but it is very difficult to keep completely adiabatic conditions. Considering that the heat transfer

is slow process, a rapid change of thermodynamic state may be approximately taken as the adiabatic process.

We performed some experiments on the relationship between temperature variation and elastic deformation of rock materials [26,28,29,40–45]. Some other studiers also performed some similar experiments [46,47]. In this paper, we carried out another experimental study using different rock samples and more advanced equipment. The study consisted of a uniaxial compression experiment and two biaxial compression experiments.

3.1. Equipment

Temperature was measured with an infrared camera, ImageIR 8800 (Made in InfraTec Company, Dresden, Germany), with the spectral range of 8~12 μm, a frame size of 640 × 512 pixels, and a temperature resolution of less than 25 mK. Temperature measuring ranged from 0 to 40 degrees Celsius (namely 273–313 K). We used the average temperature of the entire surface of the sample minus the change in ambient temperature as an estimate of the sample temperature. This calculation was used to suppress noise and eliminate the effects of ambient temperature variations. During testing, we tried to keep the room temperature stable. A biaxial electro-hydraulic servo pressure was used to load samples. The loading system used in the experiment had good control performance; as a result, the expected mechanical information could be easily obtained, which is clearly shown from the loading data (Figures 1–3). Similar good control performances of the loading system can also be found in our previous papers (e.g., [30,48]).

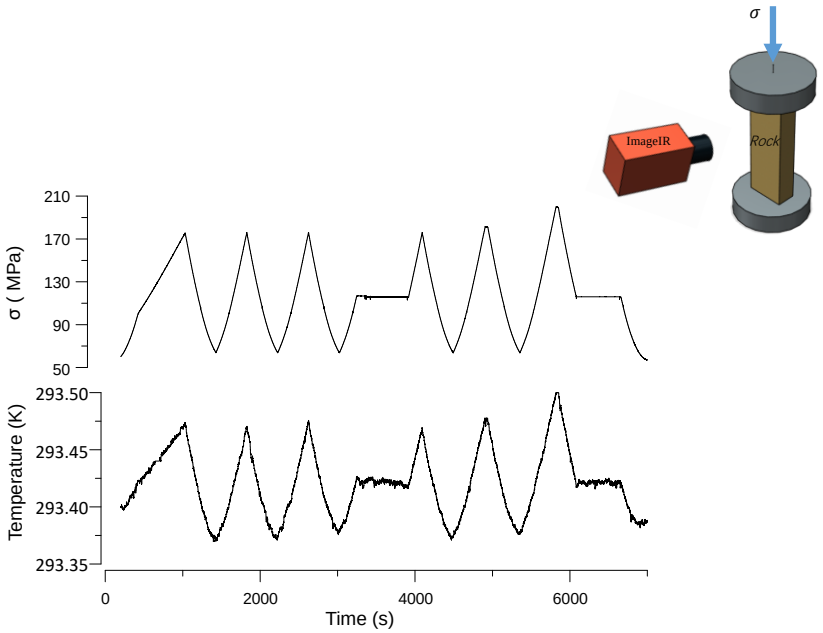

Figure 1. Variation in temperature during the uniaxial test on granite diorite.

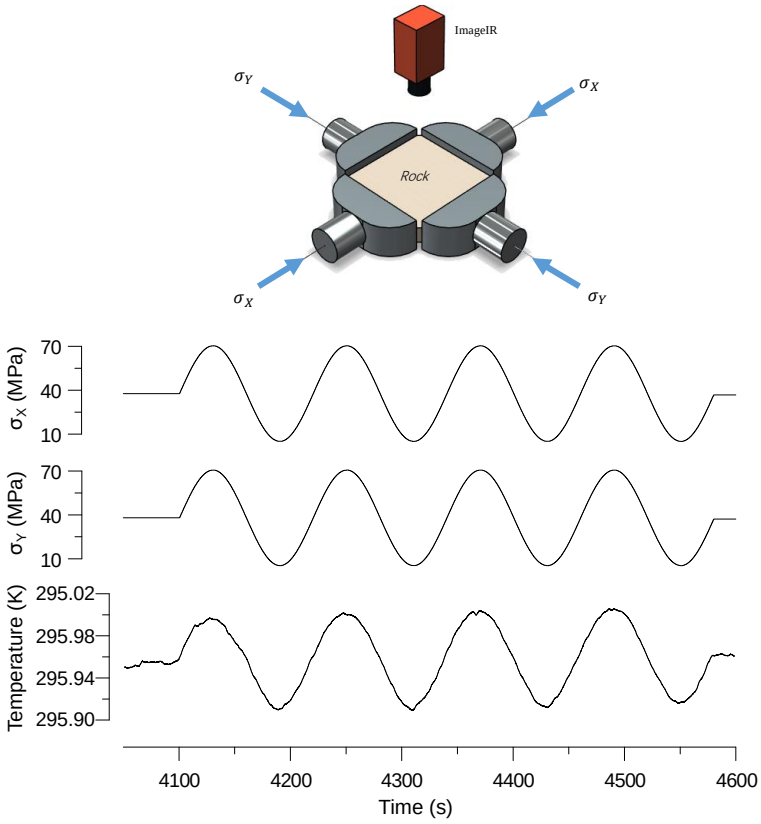

Figure 2. Variation in temperature during the biaxial test with in-phase loading on granite diorite.

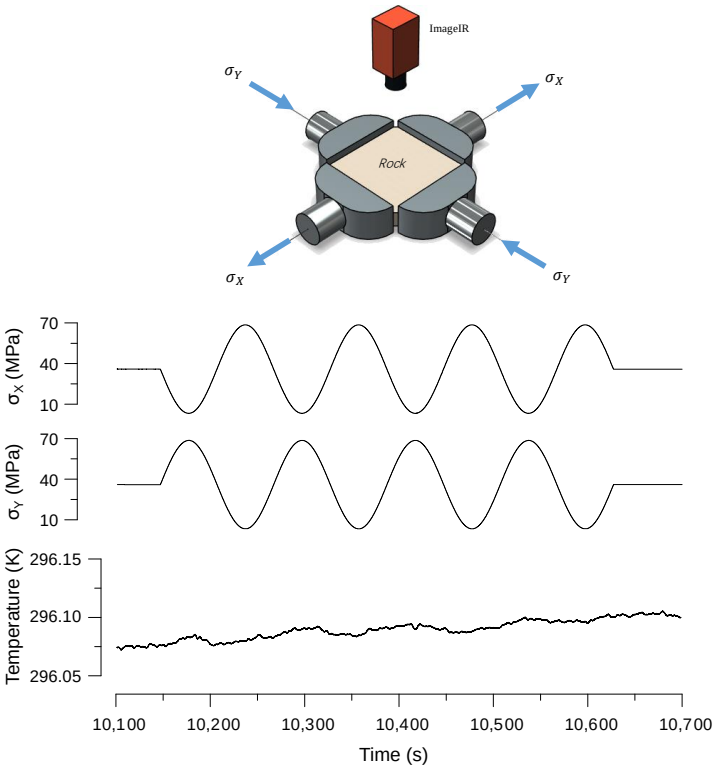

Figure 3. Variation in temperature during the biaxial test with out-of-phase loading on granite diorite.

Periodic loading was used in our experiment, which is easy to identify and can help to judge the heat loss in the environment by the temperature fluctuations in different periods. The excellent consistency of the periodic temperature fluctuations from each group of

experiments, which is shown in the following experimental results, indirectly confirms that the temperature observation actually met adiabatic conditions.

3.2. The Second Experiment

The second experiment was a simultaneous biaxial compression experiment. The rock sample was a granite diorite rectangular cuboid, with a size of 300 mm × 300 mm × 50 mm. The sample was loaded simultaneously in the x direction and y direction with a pattern of load control, while it remained free in the z direction. For the first stage, the specimen was loaded synchronously in the x and y directions, in-phase, until the stress was monotonically up to 40 MPa, and then the load remained constant. For the second stage, an additional sine-wave load, in-phase, was synchronously applied to the specimen in the x and y directions. These loads had the same period and amplitude in the x and y directions, as shown in Figure 2.

3.3. The Third Experiment

The third experiment is an asynchronous biaxial compression experiment. The samples were the same ones used in the second experiment. This experiment was applied to the load with out-of-phase loading and unloading, in which the specimen was loaded in the x direction and unloaded in y direction, or vice versa. At first, the specimen was also loaded monotonically and synchronously to 40 MPa and kept at this stress level in the x and y direction. Then, an additional load with out-of-phase sinewave was applied to the specimen. These loads had the same period and amplitude in the x and y directions, as shown in Figure 3.

As shown in Figures 2 and 3, when the specimen was loaded synchronously in the x and y directions, the deviator stress was equal to zero, and the mean stress varied with the load. The temperature varied with the load. When the test was applied by out-of-phase loading, the deviator stress varied with the load, but the mean stress remained constant. The temperature almost did not vary with the load. These results are accordant with the theoretical expectation mentioned above. Additionally, there was a little trend of temperature increase when the specimen was loaded with out-of-phase loading. A possible reason for this is that the specimen was not completely elastically deformed under the out-of-phase loading and thus there exists some irreversible temperature change. Even though this agrees with the fact that the deviator stress easily produces the plastic deformation, there could be the other reasons, i.e., cyclic loading, emissivity change, environment, or their combination, etc.

4. Field Exploration: The Case of the Thrust Fault

How to apply the above theory and experimental results to field analysis is also a difficult task. The faults in the field are complex and diverse. From the stress state, they can be divided into three types: strike fault, normal fault and thrust fault. This paper takes the thrust fault as an example to explore.

From the above theoretical analysis and experimental results, we can conclude that the mean stress change can produce a temperature change. An earthquake on the reverse fault causes a decrease in the mean stress, which causes the temperature to fall in rock walls. In order to evaluate the temperature drop caused by the mean stress drop, a mechanical model needs to be established to understand the relationship between the two. It is also necessary to determine key model parameters such as mean stress drop, fault normal stress, and friction coefficient, which are usually difficult to obtain accurately. So, we have to return to a conceptual model. Here we at first set up a general thrust fault model. Then, based on this model, we discuss how the stress changes influence the results of temperature measurement.

4.1. The Mechanical Model of the Thrust Fault

The model used in this paper is composed of a horizontal plate of rock (Figure 4). The rock top surface is free, and the bottom surface normal stress comes from gravity. The bottom surface depth is h_b. The rock density is ρ_r. In the middle part, there is a thrust fault with the dip angle θ. The mean stress increases with the increasing depth. Subsequently, the rock is compressed horizontally, and the fault slides when the shear stress of the fault exceeds the maximum static friction strength.

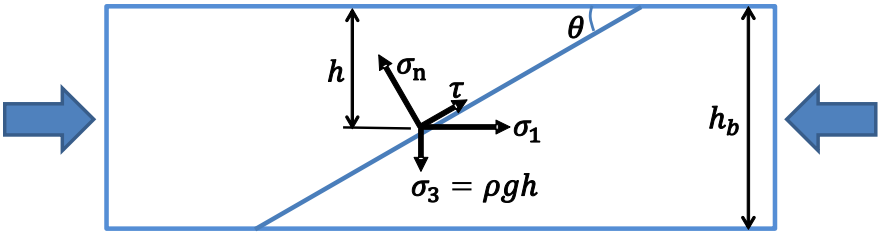

Figure 4. A simple mechanical model of the thrust fault.

As for thrust fault, the minimum principal stress σ_3 is gravity, and the maximum main stress σ_1 is horizontal and vertical to the fault strike [49]. The intermediate principal stress σ_2 is parallel to the fault strike, and along this direction the sample is infinite. According to rock mechanics, compressive stress is defined as positive value.

Assuming that the pore pressure of fluid is equal to the hydrostatic pressure, we have

$$\begin{cases} \overline{\sigma_n} = (\rho_r - \rho_w)g\overline{h} + \frac{\sigma_d}{2}(1 - \cos(2\theta)) \\ \overline{\tau} = \frac{\sigma_d}{2}\sin(2\theta) \end{cases} \quad (5)$$

where $\sigma_d = \sigma_1 - \sigma_3$ is the differential stress, $\overline{h} = h_b/2$ is the average depth, $\overline{\sigma_n}$ is the average effective normal stress of the whole fault, $\overline{\tau}$ is the average shear stress of the whole fault, ρ_r is the density of the rock, ρ_w is the density of water, and θ is the fault dip angle.

4.2. The Decrease in the Temperature in Rock Walls Due to the Mean Stress Drop Caused by Thrust Slip

The mean stress drop $\Delta\sigma_m = (\Delta\sigma_1 + \Delta\sigma_2 + \Delta\sigma_3)/3$. Since σ_3 is constant, $\Delta\sigma_3 = 0$; $\Delta\sigma_1 = \Delta\sigma_d$. As for the long fault, considering the plane strain $\varepsilon_2 = 0$, $\Delta\sigma_2 = \upsilon\Delta\sigma_d$. Additionally, we have

$$\Delta\sigma_m = (1 + \nu)\Delta\sigma_d/3 \quad (6)$$

Before an earthquake, when the fault is in the critical state of sliding, the differential stress reaches the maximum value, denoted as $(\sigma_d)_{max}$. After an earthquake, the differential stress reaches the minimal value, denoted as $(\sigma_d)_{min}$. Thus, the differential stress drop $\Delta\sigma_d = (\sigma_d)_{max} - (\sigma_d)_{min}$.

Take granite as an example. The coefficient of maximum static friction $\mu_s = 0.6$, and the coefficient of sliding friction $\mu_d = 0.2$, $\theta = 30^\circ$ (the angle of the most easy sliding when $\mu_s = 0.6$), $h_b = 10$ km, $\rho_r = 2670 kg/m^3$, $\rho_w = 1000 kg/m^3$, and $\nu = 0.25$.

When impeding an earthquake, the fault is in a critical state and the average shear stress $\overline{\tau} = \mu_s\overline{\sigma_n}$. Substituting $\overline{\tau}$ into Equation (6), gets $(\sigma_d)_{max} = 173$ MPa. Assuming that the average post-seismic shear stress is equal to the sliding friction stress $\overline{\tau} = \mu_d\overline{\sigma_n}$ and then substituting $\overline{\tau}$ into Equation (6), obtains $(\sigma_d)_{min} = 43$ MPa.

Using the Equation (6), the co-seismic mean stress drop $\Delta\sigma_m = 54$ MPa. Thus, the co-seismic temperature decrease due to stress drop is around 0.18 K.

5. Discussion

As described above, the temperature change caused by earthquakes on a thrust fault can reach 0.18 K, which is under the observable accuracy of satellite thermal infrared remote sensing. On the other hand, the differences in thermal physical properties between the solid

Earth and the atmosphere should not be neglected for thermal process analysis. Specifically, both the heat capacity and density of the solid Earth are much larger than those of the atmosphere. For example, the density and specific heat of granite are 2600 kg/m^3 and 0.82 k J/(kg.K), respectively [41]. The specific-pressure specific heat capacity, the constant-volume specific heat capacity, and the density of air are 1.004 kJ/(kg.K), 0.717 kJ/(kg.K), and 1.29 kg/m^3, respectively. Accordingly, the solid Earth's heat capacity is 1650 or 2305 times greater than that of the atmosphere when calculated with the air specific pressure and heat capacity. In the following section, we chose the lower value, namely 1650. Since the heat capacity of the solid Earth is much larger than that of the air, the influence of heat changes caused by small changes in temperature within the solid Earth cannot be ignored.

If a temperature change within the crust lasts long enough, this change may have a significant impact on the land surface temperature. Although co-seismic slip may cause a large range of temperature changes, only the heat change within the shallow crust may affect the shallow atmosphere through heat exchange in a short period of time (such as 10 days before and after an earthquake). With the reference that the influence depth of the daily-period air temperature on the shallow crust is about 1 m, we took 1–2 m of crustal depth for calculations in this paper. From the energy point of view, when the changes in temperature in the shallow crust (1–2 m in depth) reach 0.18 K, these changes may cause a change in heat that is equivalent to changes in atmospheric temperature (100 m in depth) of 3.0–6.0 K. This magnitude of temperature change is observable by the thermal infrared satellite.

Objectively, the thermal infrared information received by the satellite from the land surface thermal radiation is modified by the atmosphere, including non-tectonic factors such as a large number of complex meteorological factors. Three aspects should be considered before analyzing thermal anomalies based on satellite remote sensing information: (1) non-tectonic factors, such as atmospheric influences and solar influences; (2) intuitively speaking, the earthquake-related thermal information should have a co-seismic response since the co-seismic stress change is the largest stress change during a seismic cycle; and (3) repeatability of phenomena should be considered, i.e., the same phenomenon can be observed on different satellites. By doing these, we selected two land surface temperature products from MODIS/Aqua and MODIS/Terra to analyze thermal anomalies of two thrust earthquakes (the Wenchuan Mw 7.9 earthquake in Sichuan, China on 12 May 2008 and the Gorkha Mw 7.9 earthquake in Nepal on 25 April 2015) [50,51]. The results showed significant co-seismic cooling in both earthquakes. In particular, the spatial distribution of the co-seismic cooling response of the Wenchuan Mw 7.9 earthquake is consistent with the spatial characteristics obtained by other geodetic methods such as GPS [52]. This means that co-seismic thermal responses contain mechanical information and can be used to explore the relationship between mechanical changes and temperature responses.

Figure 5 shows the co-seismic land surface temperature along the profile perpendicular to the seismogenic fault (AB) of the Wenchuan Mw 7.9 earthquake, which was obtained by satellite. ΔT is the co-seismic temperature drop, 5.8 °C or 5.8 K, which is in accordance with those of the above-mentioned co-seismic temperature decreases; D is the cooling width, representing the range of co-seismic stress release. D is consistent with the range of deformation measured by other geodetic methods such as GPS [50,52], indicating that the co-seismic temperature drop has clear mechanical significance. For more details, please refer to the literature [50].

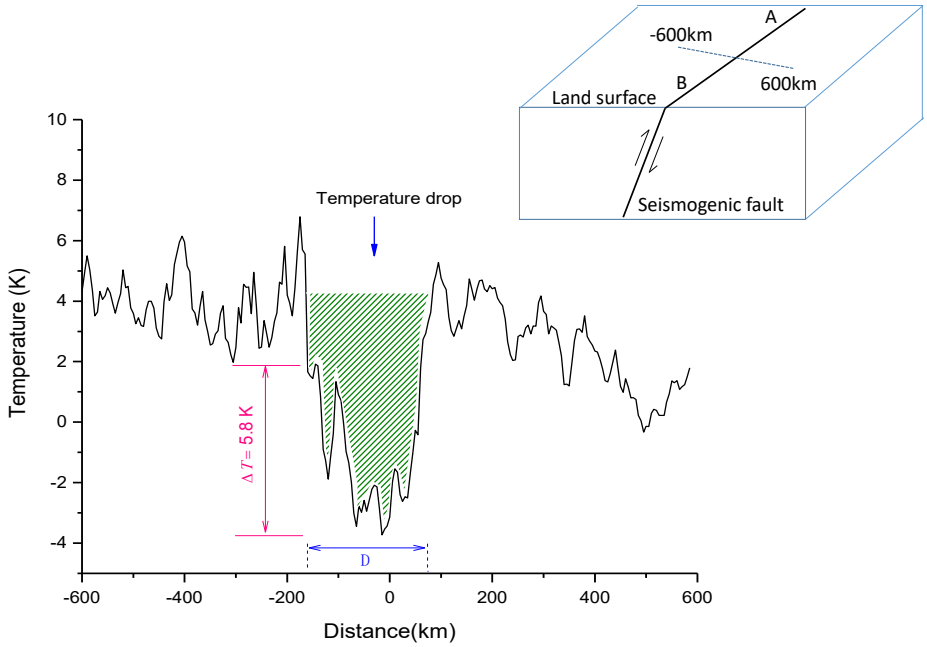

Figure 5. The spatial profile of co-seismic land surface temperature perpendicular to the seismogenic fault (AB) of the 2008 Mw 7.9 Wenchuan earthquake obtained by satellite (Revised from [50]. Note: the background land surface temperature was abstracted).

6. Conclusions

(1) The temperature change during the adiabatic elastic deformation is only related to the mean stress and independent of the deviator stress. For rock materials, the temperature rises (drops) as the mean stress increases (decreases) (compressive stress condition is taken as positive). According to Equation (4), it is convenient to obtain the relationship between the temperature response and the change in stress. Specifically, the change in temperature is 3.3 mK as a response to a change in mean stress of 1 MPa for granite.

(2) The theoretical results were verified through laboratory experiments in rock samples. Temperature was measured by an infrared camera with a spectral range of 8~12 μm. This implies that temperature change caused by stress variation can be detected in laboratory with thermal infrared radiation.

(3) The magnitude of the co-seismic temperature response can be estimated based on the co-seismic mean stress change. For thrust faulting, the co-seismic mean stress drop around the fault is about 54 MPa, and the corresponding temperature drop is about 0.18 K. From the energy point of view, the changes in temperature in the shallow crust may cause a change in heat that is equivalent to the changes in atmospheric temperature with values of 3.0–6.0 K, which are in accordance with the magnitude of the temperature anomaly obtained by the satellite thermal infrared remote sensing.

In addition, the temperature change caused by stress variation may involve the whole focal area, which has characteristics of regional distribution and is conducive to satellite observation. This means that temperature change caused by stress variation can provide a quantitative explanation of the earthquake-related satellite thermal infrared anomaly.

Author Contributions: Conceptualization, P.L. and S.C.; methodology, P.L.; software, P.L.; validation, Q.L. and J.F.; formal analysis, P.L., S.C. and Q.L.; investigation, Y.G., Y.R., Y.Z.; resources, Y.G., Y.R.; data curation, P.L.; writing—original draft preparation, P.L.; writing—review and editing, P.L. and S.C.; visualization, P.L.; supervision, P.L.; project administration, S.C.; funding acquisition, S.C. All authors have read and agreed to the published version of the manuscript.

Funding: This work Basic Research Funds from the Institute of Geology, China Earthquake Administration (Grant No. IGCEA1815), the National Key Research and Development Program of China (Grant No. 2019YFC1509202).

Data Availability Statement: Not applicable.

Acknowledgments: The work was done under the leadership of Jin Ma who passed away on 12 August 2018 after the manuscript had been finished. Thanks are owed to Yongsheng Zhou, Shengli Ma, Changrong He and Xinjian Shan, who provided helpful support for this work. We also thank two anonymous reviewers for their critical reviews and for improving the manuscript.

Conflicts of Interest: The authors declare no conflict of interest.

References

1. Gorny, V.I.; Sal'Man, A.G.; Tronin, A.A.; Shilin, B.V. Outgoing infrared radiation of the earth as an indicator of seismic activity. *Proc. Acad. Sci. USSR* **1988**, *301*, 67–69.
2. Qiang, Z.; Xu, X.; Dian, C. Satellite infrared thermos-anomaly: Earthquake imminent precursor. *Chin. Sci. Bull.* **1990**, *35*, 1324–1327.
3. Tronin, A.A. Satellite thermal survey—A new tool for the studies of seismoactive regions. *Int. J. Remote Sens.* **1996**, *17*, 1439–1455. [CrossRef]
4. Ouzounov, D.; Freund, F.T. Mid-infrared emission prior to strong earthquakes analyzed by remote sensing data. *Adv. Space Res.* **2004**, *33*, 268–273. [CrossRef]
5. Tramutoli, V.; Cuomo, V.; Filizzola, C.; Pergola, N.; Pietrapertosa, C. Assessing the potential of thermal infrared satellite surveys for monitoring seismically active areas: The case of Kocaeli (Izmit) earthquake, August 17, 1999. *Remote Sens. Environ.* **2005**, *96*, 409–426. [CrossRef]
6. Pulinets, S.; Ouzounov, D.; Karelin, A.; Boyarchuk, K.; Pokhmelnykh, L. The physical nature of thermal anomalies observed before strong earthquakes. *Phys. Chem. Earth Parts A/B/C* **2006**, *31*, 143–153. [CrossRef]
7. Blackett, M.; Wooster, M.; Malamud, B. Exploring land surface temperature earthquake precursors: A focus on the Gujarat (India) earthquake of 2001. *Geophys. Res. Lett.* **2011**, *38*, L15303. [CrossRef]
8. Bhardwaj, A.; Singh, S.; Sam, L.; Bhardwaj, A.; Martín-Torres, F.J.; Singh, A.; Kumar, R. MODIS-based estimates of strong snow surface temperature anomaly related to high altitude earthquakes of 2015. *Remote Sens. Environ.* **2017**, *188*, 1–8. [CrossRef]
9. Jiao, Z.-H.; Zhao, J.; Shan, X. Pre-seismic anomalies from optical satellite observations: A review. *Nat. Hazards Earth Syst. Sci.* **2018**, *18*, 1013–1036. [CrossRef]
10. Ahmad, N.; Barkat, A.; Ali, A.; Sultan, M.; Rasul, K.; Iqbal, Z.; Iqbal, T. Investigation of Spatio-temporal Satellite Thermal IR Anomalies Associated with the Awaran Earthquake (Sep 24, 2013; M 7.7). Pakistan. *Pure Appl. Geophys.* **2019**, *176*, 3533–3544. [CrossRef]
11. Bhardwaj, A.; Singh, S.; Sam, L.; Joshi, P.K.; Bhardwaj, A.; Martín-Torres, F.J.; Kumar, R. A review on remotely sensed land surface temperature anomaly as an earthquake precursor. *Int. J. Appl. Earth Obs. Geoinf.* **2017**, *63*, 158–166. [CrossRef]
12. Carbone, V.; Piersanti, M.; Materassi, M.; Battiston, R.; Lepreti, F.; Ubertini, P. A mathematical model of lithosphere–atmosphere coupling for seismic events. *Sci. Rep.* **2021**, *11*, 8682. [CrossRef] [PubMed]
13. Cicerone, R.D.; Ebel, J.E.; Britton, J. A systematic compilation of earthquake precursors. *Tectonophysics* **2009**, *476*, 371–396. [CrossRef]
14. Jiao, Z.; Shan, X. Pre-Seismic Temporal Integrated Anomalies from Multiparametric Remote Sensing Data. *Remote Sens.* **2022**, *14*, 2343. [CrossRef]
15. Jiao, Z.-H.; Shan, X. Statistical framework for the evaluation of earthquake forecasting: A case study based on satellite surface temperature anomalies. *J. Asian Earth Sci.* **2021**, *211*, 104710. [CrossRef]
16. Jiao, Z.-H.; Shan, X. Consecutive statistical evaluation framework for earthquake forecasting: Evaluating satellite surface temperature anomaly detection methods. *J. Asian Earth Sci. X* **2022**, *7*, 100096. [CrossRef]
17. Tronin, A.A. Satellite remote sensing in seismology. A review. *Remote Sens.* **2010**, *2*, 124–150. [CrossRef]
18. Saraf, A.K.; Rawat, V.; Choudhury, S.; Dasgupta, S.; Das, J. Advances in understanding of the mechanism for generation of earthquake thermal precursors detected by satellites. *Int. J. Appl. Earth Obs. Geoinf.* **2009**, *11*, 373–379. [CrossRef]
19. Qiang, Z.J.; Kong, L.C.; Wang, Y.P. Earth gas emission, infrared thermo-anomaly and seismicity. *Chin. Sci. Bull.* **1992**, *24*, 2259–2262.
20. Freund, F. Pre-earthquake signals-Part I: Deviatoric stresses turn rocks into a source of electric currents. *Nat. Hazards Earth Syst. Sci.* **2007**, *7*, 535–541. [CrossRef]
21. Freund, F. Pre-earthquake signals-Part II: Flow of battery currents in the Crust. *Nat. Hazards Earth Syst. Sci.* **2007**, *7*, 543–548. [CrossRef]
22. Geng, N.G.; Cui, C.Y.; Deng, M.D. Remote sensing detection of rock fracturing experiment and the beginning of remote rock mechanics (in Chinese). *Acta Seism. Sin.* **1992**, *14*, 645–652.

23. Wu, L.; Cui, C.; Geng, N.; Wang, J. Remote sensing rock mechanics (RSRM) and associated experimental studies. *Int. J. Rock Mech. Min. Sci.* **2000**, *37*, 879–888. [CrossRef]
24. Yin, J.Y.; Fang, Z.F.; Qian, J.D.; Deng, M.D.; Geng, N.G.; Hao, J.S.; Wang, Z.; Ji, Q.Q. Research on the application of infrared remote sensing in earthquake prediction and its physical mechanism. *Earthq. Res. China* **2000**, *16*, 140–148.
25. Ouzounov, D.; Liu, D.; Kang, C.; Guido, C.; Menas, K.; Patrick, T. Outgoing long wave radiation variability from IR satellite data prior to major earthquakes. *Tectonophysics* **2007**, *431*, 211–220. [CrossRef]
26. Chen, S.; Liu, P.; Guo, Y.; Liu, L.; Ma, J. An experiment on temperature variations in sandstone during biaxial loading. *Phys. Chem. Earth Parts A/B/C* **2015**, *85–86*, 3–8. [CrossRef]
27. Liu, J.; Chen, J.I.; Zhang, J.Y.; Zhang, P.Z.; Wei, W. Tectonic setting and general features of coseismic rupture of the 25 April, 2015 Mw 7.8 Gorkha Nepal earthquake (in Chinese). *Chin. Sci. Bull.* **2015**, *60*, 2640–2655. [CrossRef]
28. Yang, X.; Lin, W.; Tadai, O.; Zeng, X.; Yu, C.; Yeh, E.-C.; Li, H.; Wang, H. Experimental and numerical investigation of the temperature response to stress changes of rocks. *J. Geophys. Res. Solid Earth* **2017**, *122*, 5101–5117. [CrossRef]
29. Yang, X.; Lin, W.; Yeh, E.C.; Xu, H.; Xu, Z. Analysis on the mechanisms of coseismic temperature negative anomaly in fault zones. *Chin. J. Geophys.-Chin. Ed.* **2020**, *63*, 1422–1430.
30. Chen, S.; Guo, Y.; Liu, P.; Zhuo, Y.; Wang, K.; Ma, J. Theoretical and experimental investigations on temperature variations in granodiorite with a hole during biaxial loading and its potential implications for monitoring changes in the crustal stress. *Geophys. J. Int.* **2018**, *215*, 996–1002. [CrossRef]
31. Huang, J.W.; Liu, S.; Gao, X.; Yang, Z.C.; Ni, Q.; Wu, L.X. Experimental study of the thermal infrared emissivity variation of loaded rock and its significance. *Remote Sens.* **2018**, *10*, 818–834. [CrossRef]
32. Liu, X.X.; Wu, L.; Zhang, Y.; Wang, S.; Yao, X.L.; Wu, X.Z. The characteristics of crack existence and development during rock shear fracturing evolution. *Bull. Eng. Geol. Environ.* **2020**, *80*, 1671–1682. [CrossRef]
33. Zhang, K.; Li, N.; Liu, W.; Xie, J. Experimental study of the mechanical, energy conversion and frictional heating characteristics of locking sections. *Eng. Fract. Mech.* **2020**, *228*, 106905. [CrossRef]
34. Mineo, S.; Pappalardo, G.; Rapisarda, F.; Cubito, A.; Di Maria, G. Integrated geostructural, seismic and infrared thermography surveys for the study of an unstable rock slope in the Peloritani Chain (NE Sicily). *Eng. Geol.* **2015**, *195*, 225–235. [CrossRef]
35. Yasuyuki, K.; Jim, M.; Ryo, F.; Hisao, I.; Takashi, Y.; Setsuro, N.; Ma, K.F. Heat signature on the Chelungpu fault associated with the 1999 Chi-Chi, Taiwan earthquake. *Geophys. Res. Lett.* **2006**, *33*, 70–84.
36. Fulton, P.M.; Toczko, S. Low coseismic friction on the Tohoku-Oki fault determined from temperature measurements. *Science* **2013**, *342*, 1214–1217. [CrossRef]
37. Wojnar, R. Thermodynamics of solids with a state equation. *J. Theor. Appl. Mech.* **1999**, *37*, 809–827.
38. Hsieh, J.S. *Principles of Thermodynamics*; McGraw-Hill Inc.: New York, NY, USA, 1975.
39. Robertson, E.C. Thermal Properties of Rocks. *USGS Open-File Rep.* **1988**, *1988*, 1–106.
40. Chen, S.Y.; Liu, L.; Liu, P.; Ma, J.; Ghen, G. Theoretical and experimental study on relationship between stress-strain and temperature variation. *Sci. China Ser. D Earth Sci.* **2009**, *52*, 1825–1834. [CrossRef]
41. Liu, P.; Chen, S.; Liu, L.; Chen, G.; Ma, J. An experiment on the infrared radiation of surficial rocks during deformation. *Seismol. Geol.* **2004**, *26*, 502–511.
42. Liu, P.; Ma, J.; Liu, L.; Ma, S.; Chen, G. An experimental study on variation of thermal fields during the deformation of a compressive en echelon fault set. *Prog. Nat. Sci.* **2007**, *17*, 298–304.
43. Ma, J.; Liu, L.; Liu, P.; Ma, S. Thermal precursory pattern of fault unstable sliding:An experimental study of en echelon faults. *Chin. J. Geophys.* **2007**, *50*, 1141–1149. [CrossRef]
44. Ma, J.; Ma, S.; Liu, L.; Liu, P. Experimental study of thermal and strain fields during deformation of en enchelon faults and its geological implications. *Geodyn. Tectonophys.* **2010**, *1*, 24–35. [CrossRef]
45. Ren, Y.; Liu, P.; Ma, J.; Chen, S. Experimental study on evolution of thermal field of en echelon fault during the meta-instability stage. *Chin. J. Geophys.* **2013**, *56*, 612–622.
46. Wu, L.; Liu, S.; Wu, Y.; Wang, C. Precursors for rock fracturing and failure—Part I: IRR image abnormalities. *Int. J. Rock Mech. Min. Sci.* **2006**, *43*, 473–482. [CrossRef]
47. Wu, L.; Wu, Y.; Liu, S.; Li, G.; Li, Y. Infrared radiation of rock impacted at low velocity. *Int. J. Rock Mech. Min. Sci.* **2004**, *41*, 321–327. [CrossRef]
48. Zhuo, Y.-Q.; Liu, P.; Guo, Y.; Chen, H.; Chen, S.; Wang, K. Cross-effects of loading rate and cumulative fault slip on pre-seismic rupture and unstable slip rate of laboratory earthquakes. *Tectonophysics* **2022**, *826*, 229266. [CrossRef]
49. Scholz, C.H. *The Mechanisms of Earthquake Faulting*; Cambridge University Press: New York, NY, USA, 2002.
50. Chen, S.Y.; Ma, J.; Liu, P.X.; Liu, L.Q.; Ren, Y.Q. Exploring the current tectonic activity with satellite remote sensing thermal information: A case of the Wenchuan earthquake. *Seismol. Geol.* **2014**, *36*, 775–793.
51. Chen, S.; Liu, P.; Feng, T.; Wang, D.; Zhang, G. Exploring Changes in Land Surface Temperature Possibly Associated with Earthquake: Case of the April 2015 Nepal Mw 7.9 Earthquake. *Entropy* **2020**, *22*, 377. [CrossRef]
52. Yang, S.-M.; Lan, Q.-G.; Nie, Z.-S.; Wang, Q.-L.; Li, H.; Liao, H.; Tan, K.; Qiao, X.-J.; Wang, Q. Coseismic displacement caused by the 2008 great Wenchuan earthquake derived from various types of geodetic data. *Chin. J. Geophys.* **2012**, *55*, 2575–2588.